Spectral Module for Photon Monte Carlo Calculations in Hypersonic Nonequilibrium Radiation

Takashi Ozawa
Postdoctoral Fellow
Aerospace Research and Development Directorate,
Japanese Aerospace Exploration Agency,
Chofu, Tokyo 182–8522 Japan
e-mail: takashi@chofu.jaxa.jp

Michael F. Modest
Distinguished Professor
Fellow ASME
Shaffer and George Professor of Engineering,
Science and Engineering Building, Rm. 392
University of California,
Merced, CA 95343
e-mail: MModest@eng.ucmerced.edu

Deborah A. Levin
Professor
Department of Aerospace Engineering,
Pennsylvania State University,
University Park, PA 16802
e-mail: dalevin@engr.psu.edu

In this paper, efficient spectral modules and random number databases are developed for atomic and diatomic species for use in photon Monte Carlo (PMC) modeling of hypersonic nonequilibrium flow radiation. To model nonequilibrium flow conditions, the quasisteady state assumption was used to generate electronic state populations of atomic and diatomic gas species in the databases. For atomic species (N and O), both bound-bound transitions and continuum radiation were included and were separately databased as a function of electron temperature and number density as well as the ratio of atomic ion to neutral number density. For the radiating diatomic species of N_2^+, N_2, O_2, and NO databases were generated for each electronic molecular electronic system. In each molecular electronic system, the rovibrational transition lines were separately databased for each electronic upper state population forming the electronic system. The spectral module for the PMC method was optimized toward computational efficiency for emission calculations, wavelength selections of photon bundles and absorption coefficient calculations in the ray tracing scheme. [DOI: 10.1115/1.4000242]

Keywords: Monte Carlo, nonequilibrium, radiation, QSS, hypersonic

1 Introduction

In recent years, there has been great interest in modeling of high-speed reentry vehicles, such as Stardust [1–3] and the upcoming Crew Exploration Vehicle [4]. In these hypersonic reentry flows, radiation effects significantly influence the prediction of the heat shield design and efficiency [5]. For Stardust reentry flows, the ratio of radiative heat flux to convective heat flux was investigated in Ref. [6], and was found to be sufficiently high for altitudes lower than 80 km (e.g., 20% at 68.9 km) that coupling between flow field and radiation calculations is required. For hypersonic reentry flows, the ions and electrons inside the shock layer lead to complicated reactions among charged and neutral particles, which affect nonequilibrium atomic and molecular energy distributions and radiation behavior. Olynick et al. [2] applied a continuum Navier–Stokes flow solver loosely coupled to radiation and material thermal ablation models to predict the Stardust reentry flows at altitudes of 43–80 km and demonstrated the importance of coupling between flow field and radiation calculations. In their work, a simplistic quasi-1D tangent slab (TS) radiative transfer equation (RTE) solver was used assuming equilibrium conditions, and the radiation calculations cannot be expected to be accurate in highly nonequilibrium conditions.

To calculate radiation in nonequilibrium flows accurately, the nonequilibrium air radiation (NEQAIR) [7] code has been developed. In the NEQAIR code, the quasisteady state (QSS) assumption is used to determine the excited state populations of nonequilibrium gas species and, therefore, is considered the best line-by-line (LBL) solver for nonequilibrium flows. However, the NEQAIR LBL code, which includes a 1D tangent slab radiative transport solver, is so expensive that the code is not suitable for radiation calculations for 2D or 3D flow fields. Thus, in the work of Sohn et al. [8], a NEQAIR-based efficient databasing scheme of emission and absorption coefficients was developed. In this database, the QSS assumption is used to generate the electronic state populations of atomic and diatomic gas species. Emission and absorption coefficients for any given flow condition and wavelength range are accurately calculated using the database and its associated interpolation schemes as compared with NEQAIR results. In Ref. [9], the new database was used together with a 1D tangent slab RTE solver and the atomic radiation field was predicted for a Stardust computational fluid dynamics (CFD) simulation. The 1D RTE solver was integrated and loosely coupled with a hypersonic CFD solver. Coupling was shown to reduce the total heat load on the vehicle by about 3.5% at peak heating conditions and decreases the shock stand-off distance by 10%.

Although the NEQAIR-based database provides a means for accurate radiation calculations in nonequilibrium conditions, the 1D tangent slab radiative transport solver is not sufficiently accurate to simulate radiation for 2D or 3D flow fields. In addition, high-resolution LBL calculations require hundreds of thousands RTE solutions and become too expensive for 2D or 3D flow fields. For such cases, the photon Monte Carlo (PMC) method is accurate and can be more efficient for strongly nongray radiation fields and has been employed for such cases [10,11]. A general discussion of the Monte Carlo method for radiative transfer can be found in standard textbooks [12]. In this method radiative transfer is modeled by allowing each cell to emit its emission energy in the form of photon bundles (rays) into random directions. In Ref. [11], direct simulation Monte Carlo (DSMC) was used to study the impact of radiation on the flow, loosely coupled with the particle-based photon Monte Carlo (p-PMC) method of Wang and Modest [10] for a Stardust reentry flow field. In the p-PMC method employed in Ref. [11], emission and absorption coefficients for atomic N and O were calculated by our new NEQAIR-based line-by-line database [8]. However, it was found that tightly coupled computations between DSMC and the p-PMC are too expensive in the presence of millions of DSMC particles. Instead, a finite volume (FV) PMC method is presently being developed and close coupling between a FV-PMC and a CFD solver appears

Contributed by the Heat Transfer Division of ASME for publication in the JOURNAL OF HEAT TRANSFER. Manuscript received December 19, 2008; final manuscript received April 24, 2009; published online December 9, 2009. Assoc. Editor: Yogesh Jaluria.

more realistic. In order to couple a CFD solver with PMC radiation calculations, the time-consumption for flow field and radiation is approximately 3% and 97%, respectively. Even in such case, the PMC simulation will consume very substantial CPU time, making an efficient implementation crucial.

To carry out strongly nongray hypersonic PMC simulations with emission and absorption coefficients from many species, each depending on a large number of flow field variables, the computational efficiency of selecting wavelengths for photon bundles (rays) and of the computation of absorption coefficients at given wavelengths for each cell or each particle is crucial. In this work, we have developed new spectral modules and an emission random number database (ERND) for the PMC method to improve its computational efficiency and to solve its storage size issues. The newly developed spectral modules and random number databases can be used for both p-PMC and FV-PMC methods. Since monatomic and diatomic gases behave in a very different manner, radiatively speaking, separate databases have been constructed for the important monatomic (N, O) and diatomic (N_2^+, N_2, O_2, NO) radiating species.

2 Modeling of Spectral Module

The RTE for nonequilibrium hypersonic flow fields in the absence of scattering [13] may be written as

$$\frac{dI_{\lambda,\text{tot}}}{ds} = \hat{s} \cdot \nabla I_{\lambda,\text{tot}} = \varepsilon_{\lambda,\text{tot}} - \kappa_{\lambda,\text{tot}} I_{\lambda,\text{tot}} \tag{1}$$

where $I_{\lambda,\text{tot}}$ is the spectral radiative intensity of all species, $\varepsilon_{\lambda,\text{tot}}$ is the (nonequilibrium) emission coefficient of all species, and $\kappa_{\lambda,\text{tot}}$ is the absorption coefficient of all species. The total emission from a given cell of volume V_{cl} is

$$E_{\text{emis,cl}} = \int_{V_{\text{cl}}} \int_0^\infty \int_{4\pi} \varepsilon_{\lambda,\text{tot}} d\Omega d\lambda dV_{\text{cl}} = 4\pi \times Q_{\text{emis,tot}} \times V_{\text{cl}} \tag{2}$$

where $Q_{\text{emis,tot}}$ is the total integrated emission energy per unit volume per steradian and is equal to the summation of $Q_{\text{emis},i}$ of all species in the cell. To calculate the total emission energy, the following cell-based variables are required:

1. four temperatures ($T_{\text{tr}}, T_{\text{rot}}, T_{\text{vib}}, T_e$) (K)
2. radiating species (N, O, N_2^+, N_2, O_2, NO) number densities (cm^{-3})
3. N^+ and O^+ ion number densities (cm^{-3})
4. electron number density n_e (cm^{-3})

In general, to simulate nonequilibrium hypersonic flows, four temperatures can be calculated separately in DSMC [1], while in CFD codes, only two or three temperature models are used [9], and T_e can be assumed to be the same as T_{vib}. In the PMC method, the RTE is solved by tracing statistical photon bundles. This implies that the total energy carried by all emitted photon bundles must be equal to $E_{\text{emis,cl}}$ as given by Eq. (2). So-called random number relations must be developed to obtain statistically meaningful locations, directions, and wavelengths of emitted bundles as explained in detail by Modest [12]. While locations and directions of photon emission are straightforward, emission wavelengths for a nonequilibrium gas mixture require special attention and are a focus of the present paper. In a hypersonic plasma, there are multiple radiating species, each with multiple dependencies. First, the emitting species for a given ray is selected, based on the ratio of emitting energies for each species. A random number R'_λ, uniformly distributed from 0 to 1, is compared with the ratio of emission energies. If

$$\frac{\Sigma_{i \le i_{\text{sp}}-1} Q_{\text{emis},i}}{Q_{\text{emis,tot}}} < R'_\lambda < \frac{\Sigma_{i \le i_{\text{sp}}} Q_{\text{emis},i}}{Q_{\text{emis,tot}}} \tag{3}$$

the index of the emitting species for the ray is i_{sp}. The random number for the wavelength selection is then adjusted

$$0 \le R_\lambda = \frac{R'_\lambda \times Q_{\text{emis,tot}} - \Sigma_{i \le i_{\text{sp}}-1} Q_{\text{emis},i}}{Q_{\text{emis},i_{\text{sp}}}} \le 1 \tag{4}$$

Following Modest [12]

$$R_\lambda = \frac{Q_{\text{emis},\lambda}}{Q_{\text{emis}}} = \frac{\int_{\lambda_{\min}}^{\lambda} \varepsilon_\lambda d\lambda}{\int_{\lambda_{\min}}^{\lambda_{\max}} \varepsilon_\lambda d\lambda} \tag{5}$$

where λ is the corresponding wavelength of photon bundle emission from the i_{sp} species. A bisection method is used to select wavelengths of photon bundles.

2.1 Construction of Atomic Database. Emission random number databases (ERND) have been developed for conditions that occur in nonequilibrium flows, based on our NEQAIR-based emission and absorption coefficient database. Details on that database can be found in the work of Sohn et al. [8]. Briefly, in the atomic database, the excitation population is calculated using the QSS model as a function of electron temperature T_e, electron number density n_e, and the ratio of ion to neutral number density n^+/n_a. In the ERND, the atomic lines for N and O are databased and accumulated emission and absorption coefficient line strengths are precalculated as a function of T_e, n_e, and n^+/n_a. N and N^+, and O and O^+, respectively, are treated as single species since they have common bound-bound (bb) lines. The translational temperature is needed to determine the Doppler broadening line shape for each atomic line. Although the Doppler line shape is used as a default setting, the broadening line shape can be switched from the Doppler to the Voigt shape.

In addition to bb transitions, there are two other transition mechanisms, which lead to changes in electronic energy levels by emission and absorption of a photon, namely, transitions from a bound state to an ionized state, called bound-free (bf) transition or vice versa and transitions between two different continuum states, called free-free (ff) transitions. Bound-free radiation occurs when the upper state is ionized and the wavelength of the transition is determined by the free electron energy. For most hypersonic reentry flows the contribution from ff transitions is negligibly small. While the contribution of ff transitions are included as an option, in the default setting of the module ff transitions are not considered. In the ERND, bb transitions are separated from bf and ff transitions.

For bb transitions, the centerline wavelength λ_k (Å) and the accumulated normalized emission coefficients are stored for each line k, which is defined as

$$Q^*_{a,\text{emis},k}(T_e, n_e, n^+/n_a) = \sum_{i \le k} \varepsilon^*_{a,i}(T_e, n_e, n^+/n_a) \tag{6}$$

i.e., the accumulated strength of all lines with $\lambda_i < \lambda_k$. The superscript $*$ denotes a normalized quantity (i.e., divided by n_a). $\varepsilon^*_{a,i}$ is the normalized emission coefficient in units of W/sr for an atomic line i and is obtained from

$$\varepsilon^*_{a,i}(T_e, n_e, n^+/n_a) = \varepsilon^{c,*}_{a,i} \times \frac{n_U}{n_a} \tag{7}$$

where $\varepsilon^{c,*}_{a,i}$ is the atomic normalized emission line strength of a bound-bound transition, which is a constant. The electronic state population, n_U, is calculated as

$$n_U = \left[F(T_e, n_e, i_U) \frac{n^+}{n_a} + G(T_e, n_e, i_U) \right] \times n_a \tag{8}$$

where i_U is an upper state electronic level between 1 and 22. $\varepsilon^{c,*}_{a,i}$, i_U, and F and G are acquired from our NEQAIR-based database,

which contains $\varepsilon_{a,i}^{c,*}$ and i_U for each bb line and the F and G functions are databased for each electronic level from one to 22 for a given set of T_e and n_e values.

For N and O, 170 and 86 atomic lines are included in the databases, respectively, and are sorted in order of increasing wavelength. Based on investigations of hypersonic reentry flow fields [1,9], the important range of the electron temperature T_e has been identified as 1000–28000 K; similarly for electron number densities n_e, as $1\times10^{13}-4\times10^{16}$ cm^{-3}. For each electronic state i_U the functions F and G have been databased for equidistant values of $T_e^{0.1}$ (70 points) and $[\log(n_e)]^{0.1}$ (50 points), which was found to provide best accuracy with a minimum number of data points.

For bb transitions, the partially integrated emission is calculated as

$$Q^*_{a,\mathrm{emis},\lambda} = \int_{\lambda_{\min}}^{\lambda} \varepsilon^*_{a,\lambda}(T_e,n_e,n^+/n_a,T_{\mathrm{tr}})d\lambda = \sum_{i\le k_1} \varepsilon^*_{a,i}(T_e,n_e,n^+/n_a) + \sum_{k_1<i\le k_2} \int_{\lambda-b_{\mathrm{hw,max}}}^{\lambda} \varepsilon^*_{a,\lambda,i}(T_e,n_e,n^+/n_a,T_{\mathrm{tr}})d\lambda = Q^*_{a,\mathrm{emis},k_1}(T_e,n_e,n^+/n_a) + \sum_{k_1<i\le k_2} \varepsilon^*_{a,i} \int_{\lambda-b_{\mathrm{hw,max}}}^{\lambda} \phi_i(\lambda)d\lambda \tag{9}$$

where $\phi(\lambda)$ is the line broadening function. In Eq. (9), first the line indices, k_1 and k_2, are selected as follows: k_1 is the maximum integer with $\lambda_{k1}<\lambda-b_{\mathrm{hw,max}}$, where $b_{\mathrm{hw,max}}$ is a maximum half width of line broadening that needs to be considered (set to a constant value of 0.4 Å) and k_2 is the maximum integer with $\lambda_{k2}<\lambda+b_{\mathrm{hw,max}}$. In other words, k_1+1 is the first line (in order of increasing λ), whose ϕ_λ is not yet totally integrated, while k_2 is the last line, which is affected at all be the integration. To determine k_1 and k_2, the number of accumulated lines from $\lambda_{\min}$ to a given wavelength is stored for 800–13,200 Å with a resolution of 0.1 Å. The arrays contain k_1 and k_2 as a function of λ, where $k_{1,\mathrm{db}}(\lambda)$ is the number of lines for which $\lambda_i<\lambda-b_{\mathrm{hw,max}}$ and $k_{2,\mathrm{db}}(\lambda)$ is the number of lines for which $\lambda_i<\lambda+b_{\mathrm{hw,max}}$.

As seen from Eqs. (7) and (8), $\varepsilon^*_{a,i}$ is proportional to n^+/n_a, and thus, the accumulated normalized emission of lines can be expressed as

$$Q^*_{a,\mathrm{emis},k} = A_k \times \frac{n^+}{n_a} + B_k \tag{10}$$

In the ERND, A_k and B_k are stored for each atomic line at all different electron temperature and number density data points.

For bf and ff transitions, partially integrated normalized emission as a function of λ, is stored for each T_e, n_e, and n^+/n_a condition. For bf and ff transitions, the considered wavelength range is $\lambda=500-6000$ Å with a resolution of $\Delta\lambda=10$ Å.

The size of the ERND, including the accumulated emission lines for bb lines, the integrated emission for bf and ff transitions and k_1 and k_2 information, is approximately 31 MB and 26 MB for N and O, respectively. In Fig. 1, the line index database k_1 and k_2-k_1 for N are shown. If k_2 is not the same as k_1 at a wavelength, integrated line broadening is applied to the last term in Eq. (9). As seen from Fig. 1, the maximum of k_2-k_1 is three and, thus, partial line broadening must be applied to at most three atomic lines. For most of the lines, we do not have to consider any overlapping of lines.

2.2 Implementation of Atomic Spectral Module. In the spectral module species indices of 1 and 2 are assigned for N and O, respectively. To utilize the atomic spectral module, one calls subroutines that read λ_i, $\varepsilon_{a,i}^{c,*}$, $F(T_e,n_e,i_U)$, and $G(n_e,T_e,i_U)$ from the database for each species [8]. The integrated emission energy

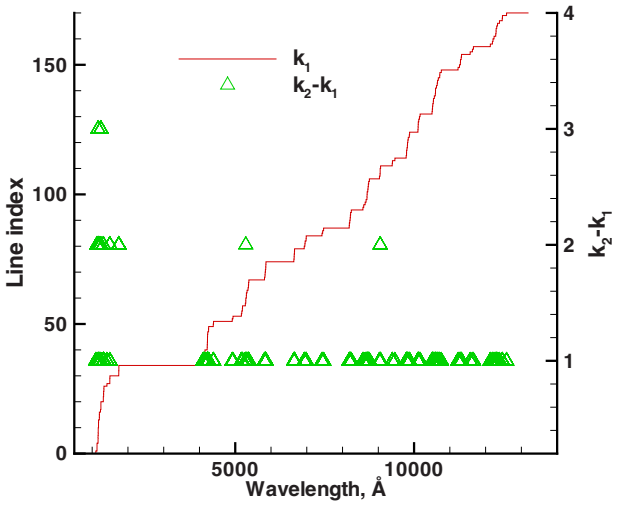

Fig. 1 Line index database of k_1 and k_2 as a function of wavelength for N

of each species per unit volume, $Q_{\mathrm{emis},i}$, is interpolated for atomic species following Eq. (9), with $Q_{\mathrm{emis}}=n_a\times Q^*_{\mathrm{emis}}$. For atomic species, T_e, n_a, n_a^+, and n_e must be known to calculate the integrated emission energy. Next, a bisection method is used to select a wavelength following Eq. (5). To this purpose a two-stage process is applied, a coarse preselection, followed by a correction. For both bb and continuum transitions, a spline interpolation scheme is used to determine the normalized emission coefficient at a given T_e and n_e. For a given n^+/n_a, the linear dependence is applied. To reduce the CPU time for spline interpolation calculations, we use linear interpolation for the preselection of wavelength.

The bisection method is used to find the resulting line (e.g., between 1 and 170 for N). In the preselection, we only consider accumulated bb line strengths and continuum contributions that are calculated using linear interpolation for T_e and n_e and n^+/n_a. Line broadening is not applied in the preselection calculations. First the line index k is identified where k with $Q^*_{a,\mathrm{emis},k}/Q^*_{a,\mathrm{emis}}<R_\lambda$. The accumulated atomic line strength $Q^*_{a,\mathrm{emis},k}$ from $i=1$ to k is read from the ERND and $\varepsilon^*_{a,i}$ is calculated as

$$\varepsilon^*_{a,i} = Q^*_{a,\mathrm{emis},i} - Q^*_{a,\mathrm{emis},i-1} \tag{11}$$

For continuum radiation, linear interpolation is used in terms of wavelength. The contributions of bb and bf transitions are summed up at a given wavelength.

Once k has been identified, the limiting line numbers k_1 and k_2 for use in Eq. (9) are found with the aid of the pretabulated accumulated lines versus wavelength array. A more accurate wavelength is then found by the bisection method from a rearranged Eq. (9)

$$(R_\lambda Q^*_{a,\mathrm{emis}} - Q^*_{a,\mathrm{emis},k1}) = \sum_{k_1<i\le k_2} \varepsilon^*_{a,i}\bar{\phi}_i(\lambda) \tag{12}$$

where the $\bar{\phi}_i(\lambda)$ come from pretabulated array of partially integrated line broadening functions. In the case of Doppler broadening this array is a function of $|\lambda-\lambda_i|/b_D$ only. For Voigt broadening, it is a two-parameter dependence, also including the ratio of Lorentz-to-Doppler broadening widths. The bisection method is applied until a λ accurate to 10^{-3} Å is found after which linear interpolation is applied.

Since the emitted ray's energy may be absorbed by any species, the absorption coefficient of all species must be known at the emission wavelength. To this purpose, the range of line numbers $k_{\mathrm{ab},1}<i\le k_{\mathrm{ab},2}$ that can contribute to the absorption coefficient is

Table 1 Random number databases for six radiating species

Species	i_{sp}	Number of bands	Transitions
N	1	1	170 bb transitions
O	2	1	86 bb transitions
N_2^+	3	2	$N_2^+(1-)$, N_2^+ (Meinel)
N_2	4	5	$N_2(1+)$, $N_2(2+)$, N_2 (Birge–Hopfield 2), N_2 (Birge–Hopfield), N_2 (Carrol–Yoshino)
O_2	5	1	O_2 (Schumann–Runge)
NO	6	18	NO(β), NO(γ), NO(Δ), NO(ε), NO(β'), NO(γ'), NO(C-A), NO(D-A), NO(B′-B), NO(E-C), NO(F-C(3)), NO(H-C), NO(H′-C), NO(E-D(5)), NO(F-D(3)), NO(H-D), NO(H′-D), NO(IR)

determined for all species, using the k_1- and k_2-arrays employed in Eq. (9).

The absorption coefficient, $\kappa_\lambda(T_e, n_e, n^+/n_a, T_{tr})$, is then calculated from the database [8] on the fly during ray tracing. The absorption coefficient of the ith bb line κ_i can be expressed as

$$\kappa_i = \kappa_{a,i}^{c,*} n_U \left(\frac{n_L}{n_U} - 1 \right)$$

$$= \kappa_{a,i}^{c,*} n_a \left[(F(i_L) - F(i_U)) \frac{n^+}{n_a} + G(i_L) - G(i_U) \right] \quad (13)$$

For calculations, $\kappa_{a,i}^{c,*}$, F, and G are obtained from databases (see Ref. [8]). In each cell, the F and G functions are interpolated in terms of electron temperature and number density. Using the interpolated F and G functions, absorption cross sections for lines between $k_{ab,1}$ and $k_{ab,2}$ are calculated. The half-widths for line broadening for lines between $k_{ab,1}+1$ and $k_{ab,2}$ are calculated, and line broadening is applied to the selected atomic lines. The bb absorption coefficient at a given wavelength is calculated as the summation of $\kappa_{i,\lambda}$ from $k_{ab,1}+1$ to $k_{ab,2}$. The bf and ff absorption coefficients at a given wavelength are calculated separately from the database [8] and are added.

2.3 Construction of Database for Molecules. For molecular radiation, N_2^+, N_2, O_2, and NO are considered in this work. A species index is assigned for each species as follows: three for N_2^+, four for N_2, five for O_2, and six for NO. In the molecular species database the excitation population is again calculated using the QSS model as a function of temperatures T_{tr}, T_{rot}, T_{vib}, T_e, n_e, and the appropriate heavy species' number densities n_h. First, the electronic systems for each electronic transition are separated, leading to two electronic systems for N_2^+, five for N_2, one for O_2, and 18 for NO based on the NEQAIR code for a total of 26 electronic systems as summarized in Table 1. For each molecular electronic system, an expression of normalized emission line strengths for rovibrational transitions can be found in Ref. [8] and the emission coefficients can be calculated as

$$\varepsilon_{\lambda,i} = \varepsilon_{m,i}^{c,*} n_U \phi_{i,\lambda} \quad (14)$$

In the database of Sohn et al. [8], $\varepsilon_m^{c,*}$, a constant, is stored for each rovibrational line for each molecular electronic system.

The rovibrational normalized line strength, $\varepsilon_{m,i}^{RV}(T_{rot}, T_{vib})$ is defined as $\varepsilon_{m,i}/n_U^e(2J_U+1)$ and is given by

$$\varepsilon_{m,i}^{RV} = \frac{\varepsilon_{m,i}^{c,*}}{(Q_{RV})_U} \times \exp\left[-\frac{hc}{k_B} \left(\frac{G(V_U)}{T_{vib}} + \frac{F(J_U)}{T_{rot}} \right) \right] \quad (15)$$

with λ_i, $\varepsilon_{m,i}^{c,*}$, $-hcG(V_U)/k_B$, and $-hcF(J_U)/k_B$ databased [8], while the rovibrational partition function $(Q_{RV})_U$ is calculated on the fly. The emission line strength for line i can simply be expressed as

$$\varepsilon_{m,i} = n_U^{e,d}(T_{tr}, T_{rot}, T_{vib}, T_e, n_e, n_h) \times \varepsilon_{m,i}^{RV}(T_{rot}, T_{vib}) \quad (16)$$

where $n_U^{e,d}$ is defined as $n_U^e \times (2J_U+1)$ and is calculated by the QSS method as a function of T_{tr}, T_{rot}, T_{vib}, T_e, n_e, and n_h.

Similar to the atomic species in Eq. (9), the partially integrated emission for each electronic system is calculated from

$$Q_{emis,\lambda}(i_{band}) = \int_{\lambda_{min}}^{\lambda} \varepsilon_\lambda(T_e, n_e, n_a, n_a^+, T_{rot}, T_{vib}, T_{tr}) d\lambda$$

$$= n_U^{e,d}(T_e, n_e, n_a, n_a^+) \left[\sum_{i \le k_1} \varepsilon_{m,i}^{RV}(T_{rot}, T_{vib}) + \sum_{k_1 < i \le k_2} \int_{\lambda - b_{hw,max}}^{\lambda} \varepsilon_{\lambda,i}^{RV}(T_{rot}, T_{vib}, T_{tr})) d\lambda \right]$$

$$= n_U^{e,d}(T_e, n_e, n_a, n_a^+) \left[Q_{m,emis,k_1}^{RV}(T_{rot}, T_{vib}) + \sum_{k_1 < i \le k_2} \varepsilon_{\lambda,i}^{RV} \int_{\lambda - b_{hw,max}}^{\lambda} \phi_i(\lambda) d\lambda \right] \quad (17)$$

In this work, the accumulated emission line strength $Q_{m,emis,k}^{RV}(T_{rot}, T_{vib})$ is databased for each rotational and vibrational temperature in the ERND. The modified upper electronic state population $n_U^{e,d}$ is calculated on the fly for each flow condition. The overall emission at a given wavelength for each species is the summation over all molecular electronic systems. The ERND is prepared separately for each molecular electronic system. For molecular radiation there are too many rovibrational lines to save all line information for all rotational and vibrational conditions. Similar to what was shown in Fig. 1, Fig. 2 shows the line index of k_1 and k_2 as a function of wavelength for the $N_2^+(1-)$ transition molecular electronic system. For this system, the total number of lines is 122,606 and the maximum of $k_2 - k_1$ is 112 as shown in the figure. Therefore, for most of the lines, we do have to consider overlapping of lines for molecules. Instead of storing the line-by-line information, $Q_{m,emis,j_{db}}^{RV}$ is stored with a resolution of $\Delta\lambda_{j_{db}}$ for each rotational and vibrational temperature and the total number of lines for $\lambda_i < \lambda_{max}$ for each molecular electronic system is also stored. $Q_{m,emis,j_{db}}^{RV}$ is the accumulated $\varepsilon_{m,i}^{RV}$ in units of W/sr between λ_{min} and $\lambda_{j_{db}}$, where $\lambda_{j_{db}}$ is the j_{db}-th wavelength in the database (equally spaced with resolution $\Delta\lambda_{db}$). Between the data points, the emission line strength of individual lines $\varepsilon_{m,i}^{RV}$ is computed in the main PMC calculations whenever necessary. In this manner the values of k_1 and k_2 similar to the atomic case are determined. For each rotational and vibrational condition, the partition function Q_{RV}, is calculated.

As for T_e, described in the atomic database, rotational and vibrational temperatures are taken to range between 1000 and

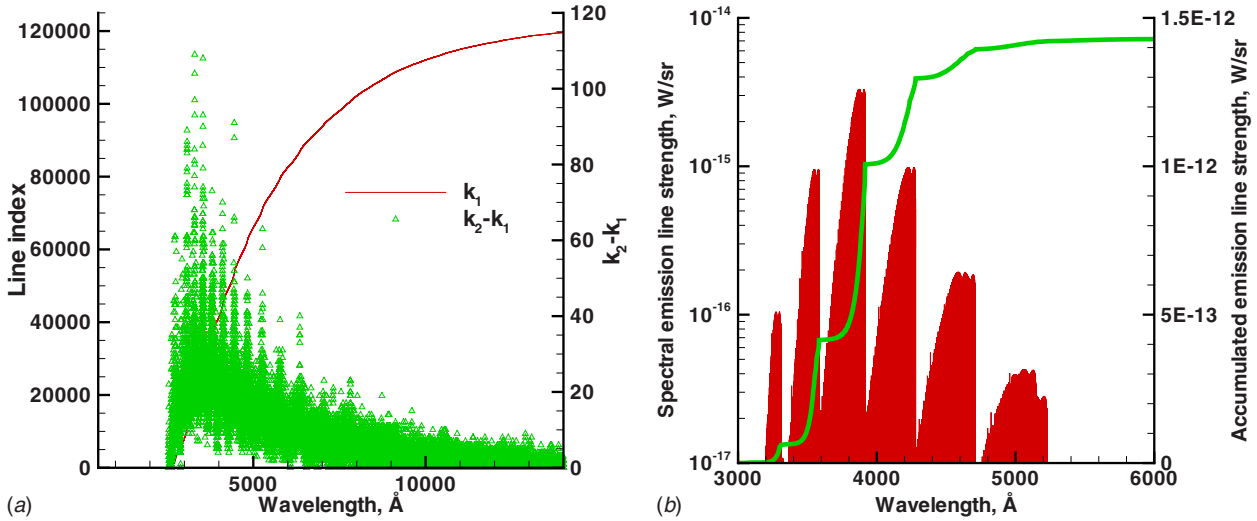

Fig. 2 Line index database of k_1 and k_2 as a function of wavelength (left) and spectral normalized emission lines and accumulated lines at temperatures of 5000 K (right) for $N_2^+(1-)$ transition molecular electronic system

28,000 K. The values have been databased for equidistant values of $T_{\text{rot}}^{0.1}$ (35 points) and $T_{\text{vib}}^{0.1}$ (35 points). For all electronic systems, a minimum wavelength $\lambda_{\min}$, a maximum wavelength $\lambda_{\max}$, and the wavelength resolution $\Delta\lambda_{\text{db}}$ are specified. At the default setting, $\lambda_{\min}$ and $\lambda_{\max}$ are 500 Å and 20,000 Å, respectively, and $\Delta\lambda_{\text{db}}$ is set to 2 Å. $\lambda_{\min}$ and $\lambda_{\max}$ can be different for each molecular electronic system but $\Delta\lambda_{\text{db}}$ is assumed to be the same constant value for all species. The information for k_1 and k_2 at a given wavelength $\lambda_{j_{\text{db}}}$, is also databased for each molecular electronic system. At the default setting, the ERND size is approximately 63 MB for each molecular electronic system. Figure 2 also shows the spectral normalized emission lines, $\varepsilon_{m,i}^{\text{RV}}$ and accumulated emission lines $Q_{m,\text{emis},j_{\text{db}}}$ for the $N_2^+(1-)$ transition molecular electronic system at temperatures equal to 5000 K. This shows an example of the ERND, indicating that for this electronic system strong lines are located between 3850 Å and 3900 Å.

2.4 Implementation of Molecular Spectral Module. To utilize the molecular spectral module, one needs to specify the molecular transition electronic systems to be considered. One sets the number of molecular species, and the number of electronic band systems. At the default setting, the numbers are set to four and 26, respectively, (the ones listed in Table 1). Each molecular electronic system to be included in the molecular radiation calculations is set individually as done in NEQAIR. The molecular line information λ_i, $\varepsilon_{m,i}^{c,*}$, $-hcG(V_U)/k_B$, $-hcF(J_U)/k_B$, $-hcG(V_L)/k_B$, and $-hcF(J_L)/k_B$ is read from our database [8] to calculate emission and absorption rovibrational line strengths.

In the main PMC calculations, one calculates electronic state populations and partition functions for each cell and each molecular species prior to ray tracing. The QSS calculations are performed by solving the four electronic states for the cell conditions on the fly. Electronic state populations $n^{e,d}$ $(T_{\text{tr}}, T_{\text{rot}}, T_{\text{vib}}, T_e, n_e, n_h)$ and partition functions $(Q_{\text{RV}})_U$ are calculated. These calculations need to be performed for all cells for both emission and absorption.

To calculate the integrated normalized emission energy per unit volume, $Q_{m,\text{emis}}^{\text{RV}}$, which is integrated from a minimum to a maximum wavelength in Eq. (17), one first obtains $Q_{m,\text{emis},j_{\text{db,max}}}^{\text{RV}}$ from the ERND and interpolates the data in terms of rotational and vibrational temperatures. The upper state level i_U, is read from our NEQAIR-based database and $Q_{m,\text{emis}}$ is multiplied by the upper state population $n_U^{e,d}$. The total integrated emission energy for the species per unit volume is calculated as the summation of $Q_{m,\text{emis}}$ over the electronic systems. The total emission energy of a cell is calculated from Eq. (2), and the number of photon bundles to be emitted from the cell is decided on. Similar to the atomic spectral module, based on the ratio of $Q_{\text{emis},i}$ for a species to $Q_{\text{emis,tot}}$ we determine, which species is emitting a photon bundle, by comparison with a random number, which is then scaled for the wavelength selection by Eq. (4).

For molecules, $Q_{m,\text{emis},j_{\text{db}}}$ in $\text{W/cm}^3/\text{sr}$ is calculated as

$$Q_{m,\text{emis},j_{\text{db}}}(i_{\text{sp}}) = \sum_{\text{bands}} n_U^{e,d} Q_{m,\text{emis},j_{\text{db}}}^{\text{RV}} \tag{18}$$

The emission wavelength is found in a two-stage process very similar to the atomic species case. First limiting line numbers k_1 and k_2 are found, in this case from $Q_{m,\text{emis},j}^{\text{RV}}$, but in $\Delta\lambda_{\text{db}}$ increments rather than for each individual line. Consequently, for the many lines of diatomic species, k_1 and k_2 may overshoot somewhat on the safe side. After k_1 and k_2 have been identified, the actual emission wavelength is found by bisection of the remainder, identical to the atomic species as indicated in Eq. (12).

Once a wavelength is selected, the absorption coefficient $\kappa_\lambda(T_{\text{tr}}, T_{\text{rot}}, T_{\text{vib}}, T_e, n_e, n_h)$, is calculated similar to the atomic species: the half width for line broadening at a given wavelength is calculated and $k_{\text{ab},1}$ and $k_{\text{ab},2}$ are read from the line index databases. Line broadening is then applied to lines between $k_{\text{ab},1}+1$ and $k_{\text{ab},2}$. The effective volumetric absorption coefficient line strength for a rovibrational transition line is given by

$$\kappa_{i,v} = \varepsilon_{m,i} \times \frac{\lambda_i^5}{2hc^2} \times \left(\frac{n_L}{n_U} - 1\right) \tag{19}$$

where

$$\frac{n_L}{n_U} = \frac{n_L^{e,d}}{n_U^{e,d}} \frac{(Q_{\text{RV}})_U}{(Q_{\text{RV}})_L} \exp\left[-\frac{hc}{k_B}\left(\frac{G(V_U) - G(V_L)}{T_{\text{vib}}} + \frac{F(J_U) - F(J_L)}{T_{\text{rot}}}\right)\right] \tag{20}$$

For rovibrational transition lines with a center wavelength of $|\lambda - \lambda_i| < 3 \times b_{\text{hw},\lambda}$, the line broadening is applied, and the absorption coefficient for the species is summed over the molecular electronic systems.

3 Results and Discussion

To demonstrate the validity and efficiency of the spectral module using the ERND, three test cases have been carried out and are presented in this section. The first case investigates the computa-

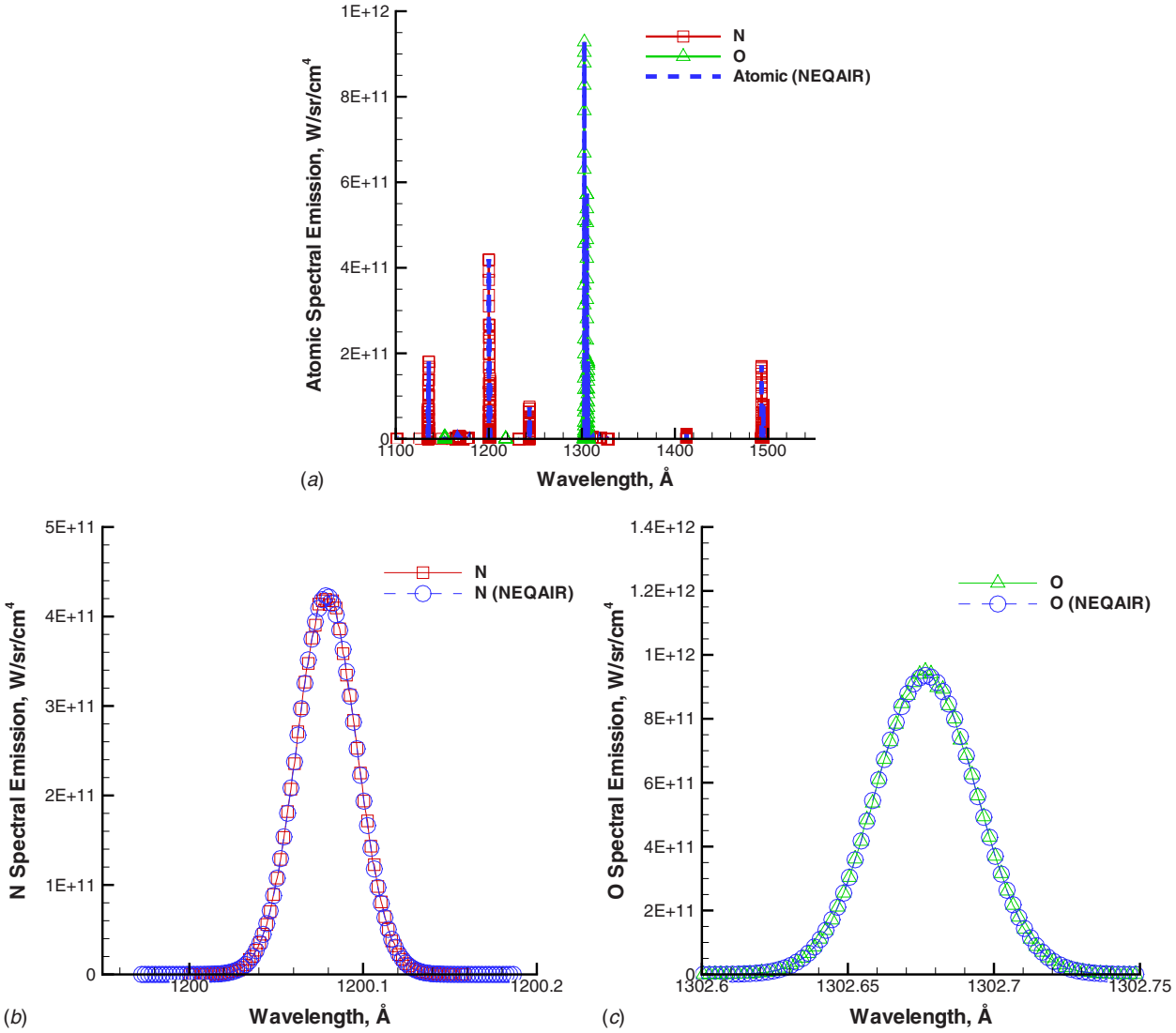

Fig. 3 Comparison of spectral emission of atomic species between spectral module and NEQAIR results

tional efficiency for wavelength selection in the PMC ray tracing scheme for both atomic and molecular spectral modules as well as the accuracy of the sampled spectral emission distributions. One arbitrary cell condition is used for emission calculations and both atomic and molecular spectral emission obtained using the spectral module are compared with NEQAIR spectral results. The second case investigates the computational efficiency to carry out a full FV-PMC calculation using a total number of 10,000 cells. Necessary steps for the FV-PMC method were considered and the CPU time was measured for each step. Finally, the FV-PMC method was used to simulate atomic radiation for a one-dimensional disk with the Stardust stagnation line flow field at 68.9 km. The flow field was obtained with a DSMC simulation and the radiative source $\nabla \cdot q$ was compared with NEQAIR tangent slab results. For these demonstrations, dual 2.4 GHz AMD Opteron Processors were used.

3.1 Accuracy and Spectral Emission Investigation. One arbitrary cell condition was used to examine the accuracy and wavelength selection efficiency of spectral modules using the ERND. Emission energies of four species (N, O, N_2^+, and N_2) were considered. Two transitions for N_2^+, $N_2^+(1-)$ and N_2^+ (Meinel), and two major transitions for N_2, $N_2(1+)$ and $N_2(2+)$, were considered, respectively. In order to have the emission energy of each species to be of the same order, the cell condition was selected as follows. Temperatures ($T_{tr}, T_{rot}, T_{vib}, T_e$) are 31,113 K, 18,027 K, 12,280 K, 14,888 K, respectively. Number densities of radiating species (N, O, N_2^+, N_2, N^+, and O^+) and electrons were 1.34×10^{16}, 1.01×10^{17}, 2.27×10^{16}, 1.75×10^{19}, 1.59×10^{14}, 1.24×10^{14}, 5.02×10^{14}, respectively. Using this cell condition, emission energies per unit volume $Q_{emis}(i_{sp})$ were calculated using the spectral module and ERND and for N, O, N_2^+, and N_2, are 790.9 W/cm^3/sr, 779.3 W/cm^3/sr, 522.1 W/cm^3/sr, and 498.9 W/cm^3/sr, respectively. 5×10^6 samples were taken using this cell condition, and the number of photon bundles for each emitting species were 1,523,992, 1,502,284, 1,002,381, 895,369, respectively. The ratio of number of samples for each species agree well with the ratio of emission energies.

Considering only atomic N and O radiation, the CPU time is approximately 220 s for 5×10^6 wavelength selections. On the other hand, for the two diatomic species N_2^+ and N_2 only, the CPU time is approximately 1600 s. For diatomic species, one needs to calculate several electronic systems for each species and, in addition, in each molecular electronic system there are many rovibrational transition lines, making them computationally more expensive than atomic species.

In Fig. 3, spectral emission of atomic species using the spectral module with the ERND is compared with NEQAIR. The photon bundle energy per sample is calculated as $Q_{emis,tot}/\Delta\lambda/N_{sample}$.

Table 2 Computational time

Step	Species	Cells	Samples	CPU time (s)
1	N, O	10,000		6
2	N_2^+, N_2	10,000		38
3	N, O, N_2^+, N_2	10,000		1
4	Selected	10,000	10	6
5	Selected	10,000	10	8

This energy is added to a wavelength column (equally spaced in $\Delta\lambda = 0.005$ Å increments), if the spectral module selects a wavelength within the column for the sample. Most selected samples were wavelengths within bb transition lines and good agreement is shown between the spectral module and the NEQAIR results. With 10×10^6 samples, the difference between the spectral module result and NEQAIR is less than 1% in the top figure. With 1×10^6 samples, the difference is approximately 5%. Detailed comparisons of spectral emission between the spectral module and NEQAIR for the strongest lines at 1200.079 Å for N and 1302.677 Å for O are also shown in the figure. Good agreement is found between the two results and line broadening (here Doppler) is well represented by the spectral module. At any selected wavelength, spectral absorption coefficients also agreed well with those of NEQAIR. Accuracy investigation was performed for the spectral emission of N_2^+ between 3000 Å and 5000 Å using the spectral module with ERND with a resolution of 0.1 Å. Since there are so many lines for molecules, more samples are required to reproduce spectral emission. For N_2^+ spectral emission, the difference between the spectral module and NEQAIR is less than 5% with 10×10^6 samples and 2% with 50×10^6 samples.

3.2 Computational Efficiency Investigation. In this subsection, the computational efficiency of FV-PMC calculations is investigated. Considering the FV-PMC method for an actual flow simulation, the total number of cells was set to 10,000. Temperatures and number densities in each cell were randomly chosen. Necessary steps for the FV-PMC method were considered and the CPU time was measured for each step. Four species (N, O, N_2^+, and N_2) were considered, and the ERNDs for these species were created. In this case, for N_2^+, two ERNDs were created for the two molecular electronic systems, $N_2^+(1-)$ and N_2^+ (Meinel). For N_2, two major electronic systems, $N_2(1+)$ and $N_2(2+)$, were selected from among five molecular electronic systems, and ERNDs were created for them. In order to employ the FV-PMC method for atomic and molecular radiation, the necessary steps are as follows:

1. F_i and G_i function interpolations
2. $n^{e,d}$ and Q_{RV} evaluations for molecules
3. total emission evaluation for four species in each cell
4. wavelength selection for ten photon bundles in each cell
5. ten absorption coefficients for each photon bundle

For each procedure, computational time was calculated and compared in Table 2. Step 1 is required to determine absorption coefficients of atomic species, and a spline interpolation scheme is used for electron temperature and linear interpolation for electron number density. In step 2 one needs to calculate the electronic excited states for each cell solving the 4×4 matrix in the QSS assumption. Also, for the partition function calculations for each electronic level, the Q_{RV} is calculated as the summation over all vibrational and rotational levels. This can be improved if Q_{RV} is databased as a functions of T_{rot} and T_{vib}. In step 4, one needs to select a wavelength for each photon bundle and the total number of photon bundles is 100,000. In step 5, the total number of absorption coefficient calculations is 1×10^6. Note that this number depends on the optical thickness of the flow and how far the photon bundle travels over cells. As one can see, the computational times for steps 3–5 are small. However, step 2 is more expensive compared with other procedures but efficient enough to allow inclusion of molecular radiation in tight coupling between the FV-PMC method and a flow field solver. During the development of the present spectral modules this test was used to identify inefficiencies in each individual schemes. The present results are for the optimized schemes described in this paper. All in all, the spectral module is so efficient that the FV-PMC method for both atomic and molecular radiation can be tightly coupled with a flow field solver.

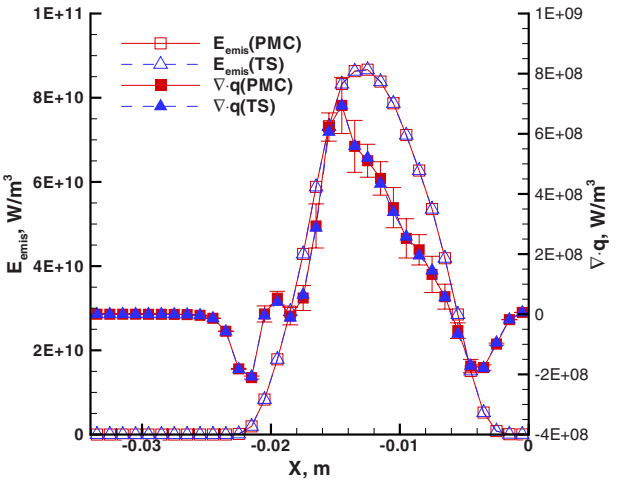

Fig. 4 Comparison of emission and $\nabla \cdot q$ of N and O gas mixture along the stagnation line between the PMC and TS (NEQAIR)

3.3 Full Flow Field Monte Carlo Simulation. A full demonstration of our spectral module was performed using the Stardust reentry flow field at 68.9 km, as calculated by a DSMC simulation [11]. The Stardust stagnation line flow field at 68.9 km mapped to a one-dimensional disk (34×5 cells) was used in the calculation to allow comparison with NEQAIR, which is limited to 1D (tangent slab) solutions and only atomic radiation was considered in the comparison [14]. Figure 4 shows combined N and O contributions to local volumetric emission $4\pi Q_{\mathrm{emis}}$ and the local radiative source

$$\nabla \cdot q = 4\pi Q_{\mathrm{emis}} - \int_0^\infty \int_{4\pi} \kappa_\lambda I_\lambda d\Omega d\lambda \tag{21}$$

It is seen that agreement is excellent, well within one standard variation in the PMC results. For the PMC method, the standard variation in $\nabla \cdot q$ is set to 0.1 and the total number of photon bundles is approximately 250×10^6. Because this case is optically very thick and almost 1D, PMC calculations are more expensive than those for NEQAIR.

4 Conclusions

New efficient spectral modules and ERNDs have been developed for both atomic and diatomic species to allow for PMC calculations of hypersonic nonequilibrium flow radiation. The QSS assumption was used to generate electronic state populations of atomic and diatomic gas species. By using the QSS assumption, the spectral module can produce accurate spectral emission coefficients for nonequilibrium flows and can select wavelengths for photon bundles efficiently. For atomic N and O, bb transitions and continuum radiation were databased separately. For the bb contribution, all accumulated bb line strengths were databased as a function of electron temperature and number density as well as the ratio of ion to neutral number density. For continuum radiation,

partially integrated emission was databased with a constant resolution wavelength. For the diatomic species N_2^+, N_2, O_2, and NO, ERNDs were generated for each electronic molecular electronic system. In each molecular electronic system, the accumulated rovibrational transition lines were divided by the electronic upper state population for the electronic system, and the normalized lines were stored with a resolution of 2 Å as a function of rotational and vibrational temperatures. To improve the computational efficiency, a bisection scheme in terms of line indices was implemented for preselection of the wavelength range and another bisection in terms of wavelength was performed after the preselection. The developed spectral module optimizes computational efficiency for emission calculations, wavelength selections of photon bundles, and absorption coefficient calculations in the ray tracing schemes used in the PMC method.

Acknowledgment

The research performed at the Pennsylvania State University was supported by NASA through Grant No. NNX07AC47A.

Nomenclature

b_{hw} = half width of the Doppler broadening, Å
c = speed of light, 2.9979×10^{10} cm/s
e = electron charge, 4.8030×10^{10} statcoul
E = energy, W
F = rotational energy quantum level for a molecule, cm^{-1}
F_i = assembled collisional and radiative coefficient of electronic state i, dimensionless
G = vibrational energy quantum level for a molecule, cm^{-1}
G_i = assembled collisional and radiative coefficient of electronic state i, dimensionless
h = Planck's constant, 6.6262×10^{-34} J s
i_{sp} = species index
I_λ = spectral intensity, $W/cm^2/sr/Å$
J = rotational quantum number, dimensionless
k = line index
k_B = Boltzmann's constant, 1.3806×10^{-23} J/K
n = number density, cm^{-3}
$n_U^{e,d}$ = modified upper electronic state population of molecule, $n_U^{e,d} = n_U^e \times (2J_U + 1)$
Q_{emis} = integrated emission coefficient, $W/cm^3/sr$
$Q_{emis,\lambda}$ = partially integrated emission coefficient, $W/cm^3/sr$
Q_{RV} = rovibrational partition function, dimensionless
R = uniform random number between 0 and 1
T = temperature, K
V_{cl} = volume of a cell, cm^3
ε_λ = emission coefficient, $W/cm^3/sr/Å$
ε_i = emission line strength at the centerline, $W/cm^3/sr$
κ_λ = absorption coefficient, cm^{-1}
κ_i = absorption coefficient line strength, dimensionless
λ = wavelength, Å
$\phi(\lambda)$ = line broadening function, $Å^{-1}$
$+$ = ion
RV = rotational and vibrational temperature dependence (divided by $n_U^{e,d}$)
$*$ = normalized quantity

References

[1] Ozawa, T., Zhong, J., and Levin, D. A., 2008, "Development of Kinetic-Based Energy Exchange Models for Non-Continuum, Ionized Hypersonic Flows," Phys. Fluids, **20**(4), p. 046102.
[2] Olynick, D., Chen, Y.-K., and Tauber, M. E., 1999, "Aerothermodynamics of the Stardust Sample Return Capsule," J. Spacecr. Rockets, **36**(3), pp. 442–462.
[3] Park, C., 2007, "Calculation of Stagnation-Point Heating Rates Associated With Stardust Vehicle," J. Spacecr. Rockets, **44**(1), pp. 24–32.
[4] Johnson, E. J., Starkey, R. P., and Lewis, M. J., 2006, "Aerodynamic Stability of Reentry Heat Shield Shapes for a Crew Exploration Vehicle," J. Spacecr. Rockets, **43**(4), pp. 721–730.
[5] Zhong, J., Ozawa, T., and Levin, D. A., 2008, "Modeling of Stardust Reentry Ablation Flows in the Near-Continuum Flight Regime," AIAA J., **46**(10), pp. 2568–2581.
[6] Ozawa, T., Zhong, J., Levin, D. A., Boger, D. A., and Wright, M., 2007, "Modeling of the Stardust Reentry Flows With Ionization in DSMC," AIAA Paper No. 2007-0611.
[7] Park, C., 1985, "Nonequilibrium Air Radiation (NEQAIR) Program: Users Manual," Ames Research Center, NASA.
[8] Sohn, I., Bansal, A., Levin, D. A., and Modest, M., 2008, "Advanced Radiation Calculations of Hypersonic Reentry Flows Using Efficient Databasing Schemes," Seattle, WA, AIAA Paper No. 2008-4091.
[9] Feldick, A. M., Modest, M., and Levin, D. A., 2008, "Closely Coupled Flowfield-Radiation Interactions for Flowfields Created During Hypersonic Reentry," 40th Thermophysics Conference, Seattle, WA, Jun. 23–26, AIAA Paper No. 2008-4104.
[10] Wang, A., and Modest, M. F., 2006, "Photon Monte Carlo Simulation for Radiative Transfer in Gaseous Media Represented by Discrete Particle Fields," ASME J. Heat Transfer, **128**(10), pp. 1041–1049.
[11] Ozawa, T., Wang, A., Modest, M., and Levin, D. A., 2008, "Development of a Coupled DSMC-Particle Photon Monte Carlo Method for Simulating Atomic Radiation in Hypersonic Reentry Flows," Seattle, WA, AIAA Paper No. 2008-3916.
[12] Modest, M. F., 2003, *Radiative Heat Transfer*, 2nd ed., Academic, New York.
[13] Park, C., 1990, *Nonequilibrium Hypersonic Aerothermodynamics*, Wiley, New York.
[14] Sohn, I., Ozawa, T., Levin, D. A., and Modest, M., 2009, "DSMC Hypersonic Reentry Flow Simulations With Photon Monte Carlo Radiation," Orlando, FL, AIAA Paper No. 2009-1566.